Journal of Marine Science and Technology

Volume 24 | Issue 4 Article 12

SIMULATION OF THE EFFECT OF BREAKWATER ON THE PROPAGATION OF SOLITARY WAVES

Ching-Piao Tsai
Department of Civil Engineering, National Chung Hsing University, Taichung, Taiwan, R.O.C,
cptsai@dragon.nchu.edu.tw

Ying-Chi Chen
Department of Civil Engineering, National Chung Hsing University, Taichung, Taiwan, R.O.C.

Chun-Jen Chen
Union-Tech Engineering Consultants Co., Taipei, Taiwan, R.O.C

Chang Lin
Department of Civil Engineering, National Chung Hsing University, Taichung, Taiwan, R.O.C.

Recommended Citation

Tsai, Ching-Piao; Chen, Ying-Chi; Chen, Chun-Jen; and Lin, Chang (2016) "SIMULATION OF THE EFFECT OF BREAKWATER ON THE PROPAGATION OF SOLITARY WAVES," *Journal of Marine Science and Technology*: Vol. 24: Iss. 4, Article 12.
DOI: 10.6119/JMST-016-0311-2
Available at: https://jmstt.ntou.edu.tw/journal/vol24/iss4/12

Journal of Marine Science and Technology, Vol. 24, No. 4, pp. 780-789 (2016)
DOI: 10.6119/JMST-016-0311-2

SIMULATION OF THE EFFECT OF BREAKWATER ON THE PROPAGATION OF SOLITARY WAVES

Ching-Piao Tsai[1], Ying-Chi Chen[1], Chun-Jen Chen[2], and Chang Lin[1]

Key words: solitary wave, breakwater, CFD, RANS, RNG, wave transformation, run up, jet-like flow, vorticity, turbulent energy dissipation.

ABSTRACT

A numerical simulation of the effect of breakwater on the propagation of solitary waves was presented in this study using CFD based on the Reynolds-averaged Navier-Stokes (RANS) equations coupled with the renormalization group (RNG) turbulent model. The wave transformation and the flow field variation of solitary waves propagating over composite breakwaters of different heights were simulated. The effect of breakwater height on the run-up of solitary waves on the slope was discussed. The simulation results revealed a jet-like flow phenomenon when solitary waves passing over breakwaters due to the water level difference between the weather and lee sides of the breakwater; additionally, significant vorticity developed at the location where jet-like flow occurred, and relatively significant turbulent energy dissipation was generated. The simulation results showed that the run-up of the solitary waves on the sloping terrain was significantly reduced with increasing breakwater height. The solitary waves reaching land was deferred by the blocking effect of the breakwater, but the wave force on the upright section of the breakwater was increased with increasing the breakwater height.

I. INTRODUCTION

In March 2011, a Richter magnitude 9.0 earthquake, named the 2011 Great East Japan earthquake, occurred in Tohoku, Japan, triggering a powerful tsunami and the run-up of a significant amount of water on land. Maximum run-up heights greater than 10 m were distributed along 500 km of coast within a direct distance (Mori and Takahashi, 2012). The tsunami caused major disasters, including damage to the Fukushima Nuclear Power Plant, which drew significant attention from around the globe. The enormous breakwater in Kamaishi Harbor, Japan, was also severely damaged, leading to nearly 1,000 deaths in Kamaishi City. The construction of the Kamaishi breakwater, which was generally regarded as the largest breakwater in the world, was completed in 2009. However, the Kamaishi breakwater was damaged because of the significant tsunami-induced hydrodynamic impacts. Therefore, understanding the hydrodynamic characteristics caused by the interaction between tsunami waves and breakwaters is beneficial to the safety design of structures.

Some researchers have suggested the use of N-waves to simulate tsunami waves (e.g., Tadepalli and Synolakis, 1994). However, in recent decades, most of the related studies have focused either on investigations of the hydrodynamic characteristics induced by the propagation of tsunami waves or on the interaction between tsunami waves and structures using solitary waves (Liu et al., 2008). There were numerous literature on the investigations of the related issues, such as for the run-up of solitary waves on plane beaches (Synolakis, 1987; Carrier et al., 2003; Li and Raichlen, 2003; Lin et al., 2014), for the tsunami run-up around islands (Liu et al., 1995; Cho et al., 1999; Choi et al., 2007), and for the interaction of solitary waves with structures (Cooker et al., 1990; Grill et al., 1994; Silva et al., 2000; Huang and Dong, 2001; Lynett et al., 2001; Lin et al., 2005; Lin and Karunarathna, 2007; Nakamura et al., 2008; Hsiao and Lin, 2010; Wu and Hsiao, 2013).

Horiguchi and Yokota (1968) discussed the failure mechanism of the Kawaragi Breakwater in the Port of Hachinohe, induced by the Tokachi Earthquake tsunami. They noted that during a tsunami, the water level difference between the weather side and leeside of the breakwater and its induced net dynamic pressure force were the main factors that led to breakwater sliding and eventual breakwater damage. According to the study conducted by Arikawa et al. (2012), there were two main causes of the damage sustained by the Kamaishi breakwater when the tsunami landed: one, the induced water level difference between the weather side and leeside of the breakwater was significant, and two, the riprap berm was scoured after the tsunami overtopping the breakwater, reducing the friction on the bottom of the gravity structure. As a result, the breakwater was no longer able to resist the force of the tsunami and eventually sustained damage. Arikawa et al. (2012) conducted open-channel flow to simulate the tsunami overflow, but failing to consider the long-

Paper submitted 10/12/15; revised 01/30/16; accepted 03/11/16. Author for correspondence: Ching-Piao Tsai (e-mail: cptsai@dragon.nchu.edu.tw).
[1] Department of Civil Engineering, National Chung Hsing University, Taichung, Taiwan, R.O.C.
[2] Union-Tech Engineering Consultants Co., Taipei, Taiwan, R.O.C.

wave effect of the tsunami.

In the present study, a numerical investigation of the effect of breakwater on the propagation of solitary waves was performed. The wave transformations and the flow field variation characteristics of solitary waves propagating over breakwaters are discussed. Breakwaters of three different heights of the upright section, in relation to the water surface, were considered, including a submerged breakwater (i.e., the top of breakwater was below the water surface), a surface breakwater (i.e., the top height of the breakwater was at the water surface) and an emerged breakwater (i.e., the top height of the breakwater was above the water surface). The effect of different breakwater heights on the variation of the hydrodynamic characteristics of the solitary waves is discussed, including the wave transformation, velocity field, turbulent energy dissipation and variation of the run-up on a slope. As the tsunami waves propagating over the breakwater, the water level difference and the wave force on the breakwater are also investigated.

II. FORMULATIONS FOR NUMERICAL SIMULATIONS

The present numerical simulation was established using the Reynolds-averaged Navier-Stokes (RANS) equations with the renormalization group (RNG) k-ε turbulent model. To model the complex geometric boundary by the fractional area/volumes obstacle representation (FAVOR) technique (Hirt and Sicilian, 1985), the general continuity and momentum equations for incompressible turbulent flows are formulated with area and volume fraction functions, which are given as

$$\frac{\partial \langle u_i \rangle A_i}{\partial x_i} = 0 \tag{1}$$

$$\frac{\partial \langle u_i \rangle}{\partial t} + \frac{1}{V_F}\langle u_j \rangle A_j \frac{\partial \langle u_i \rangle}{\partial x_j} = -\frac{1}{\rho}\frac{\partial \langle p \rangle}{\partial x_i} + \frac{1}{\rho V_F}\frac{\partial}{\partial x_j}\left[A_j(\langle \tau_{ij} \rangle + R_{ij}) \right] \tag{2}$$

wher $\tau_{ij} = 2\mu S_{ij}$ with $S_{ij} = (\partial \langle u_i \rangle / \partial x_j + \partial \langle u_j \rangle / \partial x_i)/2$, the notation of $\langle\ \rangle$ denotes the ensemble-averaged or so called time-averaged properties, u is the velocity component in the subscript direction, the subscripts = 1, 2 represent x- and z-directions, respectively, p is the pressure intensity, ρ is the fluid density, g is the gravitational acceleration, and μ is the absolute viscosity. V_F is the fractional volume open to the flow and A is the fractional area open to flow in the subscript direction. The above governing equations are reduced to standard RANS equations as both V_F and A are set to unity. The Reynolds stress term R_{ij} in Eq. (2) is expressed by

$$R_{ij} = 2\rho \nu_t S_{ij} - \frac{2}{3}\rho k \delta_{ij} \tag{3}$$

where ν_t is the eddy viscosity, k is the turbulent kinetic energy, and δ_{ij} is the Kronecker delta function such that δ_{ij} = 1 when $i = j$; δ_{ij} = 0, when $i \neq j$.

In Eq. (3), the eddy viscosity ν_t is related to the effect of the space and time distribution of the turbulent motion, which is solved here using the renormalization group method (RNG k-ε model). The RNG k-ε turbulent model was proposed by Yokhot and Orszag (1986) and makes an improvement over the k-ε model. The transport equations of the RNG k-ε model are expressed in a Cartesian coordinate system as:

$$\frac{\partial k}{\partial t} + \langle u_j \rangle \frac{\partial k}{\partial x_j} = 2\nu_t S_{ij}\frac{\partial \langle u_i \rangle}{\partial x_j} + \frac{\partial}{\partial x_j}(\alpha_k \nu_{eff}\frac{\partial k}{\partial x_j}) - \varepsilon \tag{4}$$

$$\frac{\partial \varepsilon}{\partial t} + \langle u_j \rangle \frac{\partial \varepsilon}{\partial x_j} = 2c_{\varepsilon 1}\frac{\varepsilon}{k}\nu_t S_{ij}\frac{\partial \langle u_i \rangle}{\partial x_j} + \frac{\partial}{\partial x_j}(\alpha_\varepsilon \nu_{eff}\frac{\partial \varepsilon}{\partial x_j}) - c_{\varepsilon 2}\frac{\varepsilon^2}{k} - R_o \tag{5}$$

$$\nu_t = c_\mu \frac{k^2}{\varepsilon} \tag{6}$$

$$\nu_{eff} = \nu_t \left[1 + \sqrt{\frac{c_\mu k}{\mu\sqrt{\varepsilon}}} \right]^2 \tag{7}$$

$$R_o = \frac{c_\mu \eta^3 (1 - \frac{\eta}{\eta_o})\varepsilon^2}{(1 + c_3\eta^3)k} \tag{8}$$

$$\eta = \sqrt{\frac{2k}{\varepsilon} S_{ij}\frac{\partial \langle u_i \rangle}{\partial x_j}} \tag{9}$$

where k and ε represent the turbulent kinetic energy and turbulent energy dissipation, respectively. One of the major advantages of the RNG theory is that the important turbulent coefficients are theoretically determined rather than being adjusted empirically. According to Orszag et al. (1996), the turbulence transport coefficients shown in the above equations are set to $c_{\varepsilon 1}$ = 1.42, $c_{\varepsilon 2}$ = 1.68, c_3 = 0.012, c_μ = 0.085, η_o = 4.38, α_k = 0.7194, and α_ε = 0.7194.

The numerical solutions are implemented by Flow-3D CFD (Flow Science, 2012), which utilizes a true volume of fluid (VOF) method (Hirt and Nichols, 1981) to accurately track the free water surface and models efficiently the solid geometries using the FAVOR technique. Several studies have applied Flow-3D to work successful the issues of the interaction of waves and structures, such as in Choi et al. (2007), Jin and Meng (2011) and Dentale et al. (2014). In this study, the solution of solitary wave derived from Boussinesq equations were used as the incident wave, which was expressed as:

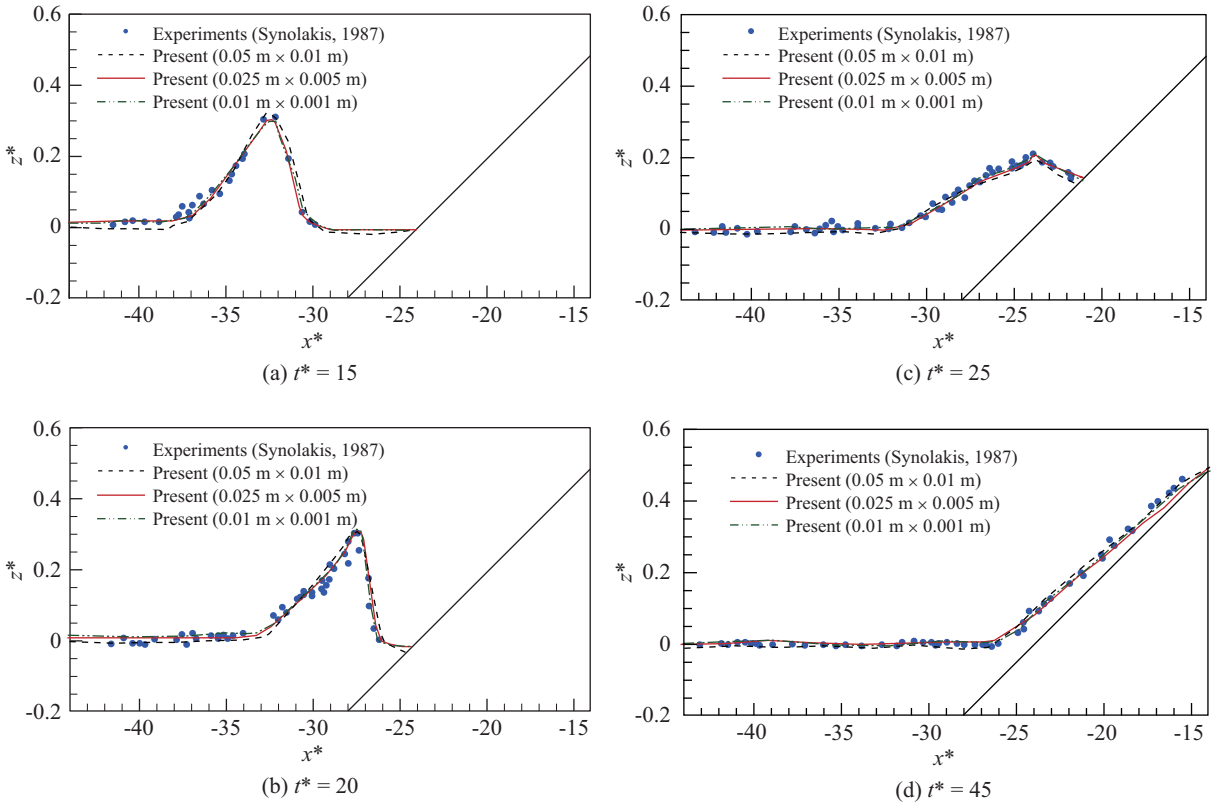

Fig. 1. The simulation results of the solitary wave transformations and their comparisons.

$$\eta(x,t) = H \operatorname{sech}^2\left[\sqrt{\frac{3H}{4h_0^3}}(x-ct)\right] \tag{10}$$

where η is the free surface elevation, h_0 the still water depth, H the wave height, and c is the wave celerity ($c=\sqrt{g(h_0+H)}$).

The initial water body was set in a static state. As for the boundary conditions, the tangent shearing stress of the free surface was set as zero; the normal stress was in equilibrium with the atmospheric pressure; and all of the solid surfaces were treated using the no-slip boundary condition. The variation of the turbulent energy and the turbulent dissipation on the free surface boundary was set as zero in the normal direction.

III. VERIFICATIONS

The experimental data by Synolakis (1987) were first used to verify the numerical simulation on solitary waves. The experimental results from Synolakis's study have been widely used in simulation verification (e.g., Lynett et al., 2002). The referenced experimental water depth (h_o) for the simulation was 0.21 m; the ratio of the wave height to water depth (H/h_o) was 0.28; and the slope of the section after the constant water depth section was 1/20. Three different computational meshes were used to validate the numerical accuracy; they are 0.05 m (x) × 0.01 m (z), 0.025 m (x) × 0.005 m (z) and 0.01 m (x) × 0.001 m (z), respectively.

Figs. 1(a)-(d) show the simulation results of the wave transformation on the slope and their comparisons. The circular points in the figure represent the experimental data from Synolakis (1987); the solid lines represent the present numerical simulation results; and the dimensionless coordinates were defined as $x^*=x/h_o$, $z^*=z/h_o$ and $t^*=t\sqrt{g/h_o}$. Fig. 1(a) shows the solitary waves approaching the slope; Fig. 1(b) shows the effect of shoaling on the solitary waves, where the wave height tended toward the maximum; and Figs. 1(c) and (d) show the run-up of the solitary waves on the slope and their maximum run-up after the solitary waves broken. A comparison among the waveform variations demonstrates that the numerical accuracy could be obtained by using the computational mesh of 0.025 m (x) × 0.005 m (z).

There were only very few experiments performed to investigate the velocity field variation during the solitary wave transformation. Lin et al. (2014) investigated the velocity field induced by a solitary wave propagating over a 1:10 slope using flow visualization techniques and high time-resolved particle image velocimetry (PIV), from which their experimental results were adopted to verify the present numerical simulation. The comparisons were performed for the conditions of wave height (H) of 2.1 cm, the water depth (h_o) of 8 cm, and wave celerity (c) of 98.0 cm/s. The grid of 0.025 m (x) × 0.005 m (z)

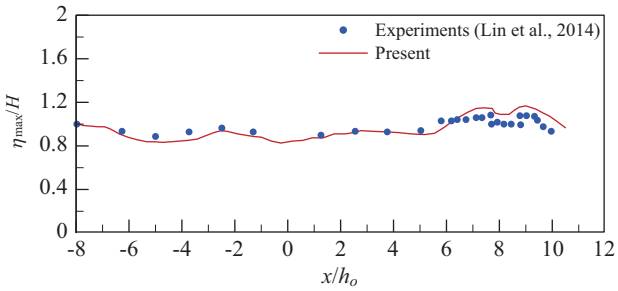

Fig. 2. Comparisons of the variations of maximum free surface elevation along a slope.

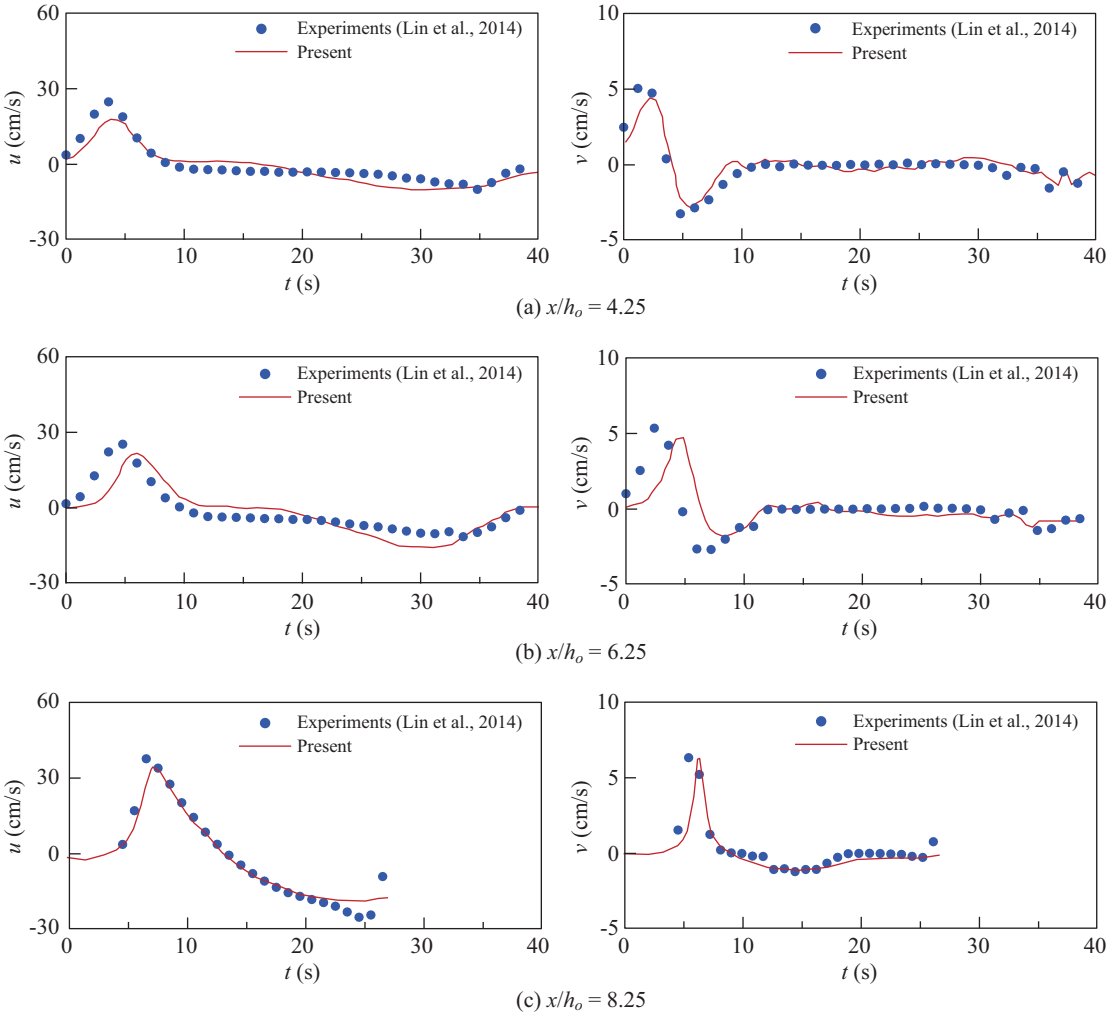

Fig. 3. Comparisons of the time variations of the ensemble-averaged horizontal and vertical velocities at $z/h_o = 0.7$ for different cross sections shown in Fig. 2.

was also applied to the numerical calculation. Fig. 2 shows good agreement between the numerical simulation and experiment of the variations of maximum free surface elevation (η_{max}) along the slope. It shows that η_{max} reaches maximum at x/h_o = 8.9 and then decays rapidly indicating where wave breaking occurs. Fig. 3 shows the time variations of the ensemble horizontal and vertical velocities (u, v) at z/h_o = 0.7 for different cross sections, which depicts good agreement between the numerical and experimental results.

The above comparisons among the variations of wave profile and velocity field demonstrate that the numerical model adopted in the present study could accurately simulate the trans-

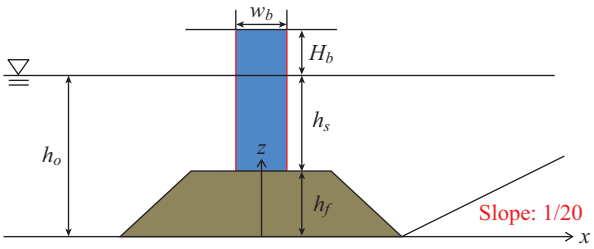

Fig. 4. A schematic diagram of the physical model for the simulation in the present study.

formation of the solitary waves.

IV. SIMULATION RESULTS AND DISCUSSION

1. Simulated Conditions

In the present study, we mainly focus on discussing the effect of different breakwater heights on the transformation of solitary waves. Fig. 4 shows the physical model, which is a composite type of breakwater consisting of a rectangular caisson and a trapezoid foundation with berm. Breakwaters of three different heights relative to the water surface were considered, including a submerged breakwater (i.e., $H_b < 0$), a surface breakwater (i.e., $H_b = 0$) and an emerged breakwater (i.e., $H_b > 0$). The height of the trapezoidal foundation of the breakwater was set as a fixed value $h_f = 0.2$ m. The depth from the still water surface to the berm was $h_s = 0.12$ m. The width of the upright caisson of the breakwater was $w_b = 0.3$ m. There were three different heights of the upright section of breakwaters, namely, $H_b = -0.04$ m, 0 m and +0.04 m. The front of the breakwater was set as a uniform water depth, $h_o = 0.32$ m, and the ratio of the wave height to water depth, H/h_o, was 0.20.

To investigate the effect of the breakwater on the run-up of solitary waves on a slope, a section with a slope of 1/20 was placed at the back of the breakwater. The length and height of the slope were 11 m and 0.55 m, respectively. In the numerical simulation, the total length of the simulated channel was set as 50 m. A single grid was used for simulation. The size of the computational grid was 0.025 m (x) × 0.005 m (z).

2. Wave Profile Transformations

Fig. 5 shows the simulated results of the surface profile transformation of the solitary waves when propagating over breakwaters of different heights. The transformation of the solitary waves with no breakwater present is also shown in the figure. Fig. 5(a) shows that when the solitary waves approached the breakwater, an asymmetric variation of the wave profile occurred. As the height of the breakwater increased, the asymmetric waveform increased, due to the blocking effect of the breakwater. After the solitary waves propagated over the breakwater (Fig. 5(b)), a significant waterfall phenomenon developed when the upright height of the breakwater (H_b) was either 0 m or +0.04 m. After the solitary waves propagated over the breakwater, a portion of the reflected waves remained at the front of the breakwater (Fig. 5(c)). Fig. 6 shows a comparison between the situation in which there was no breakwater and that in which the breakwater had a freeboard (H_b) of 0 m, as well as the run-up of the solitary waves on the slope. It can be clearly seen that after the solitary waves propagated over the breakwater, the height of the run-up on the slope decreased due to the blocking effect of the breakwater.

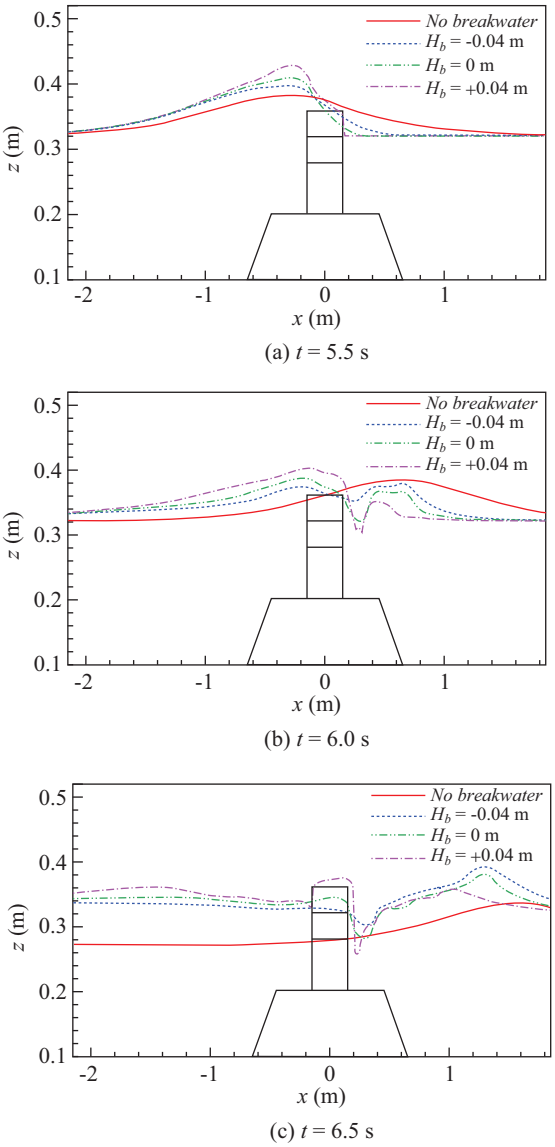

Fig. 5. A comparison among the variations of the waveforms when the solitary waves propagated over the breakwaters of different heights.

Fig. 7 shows the variation of the water levels at the weather and lee sides of the breakwater when the solitary waves passing over the breakwater. As the height of the breakwater increased, the water level difference between the weather and lee sides of the breakwater increased. This water level difference can cause significant changes of the net wave force on the upright of the breakwater (discussed in Section 4.6).

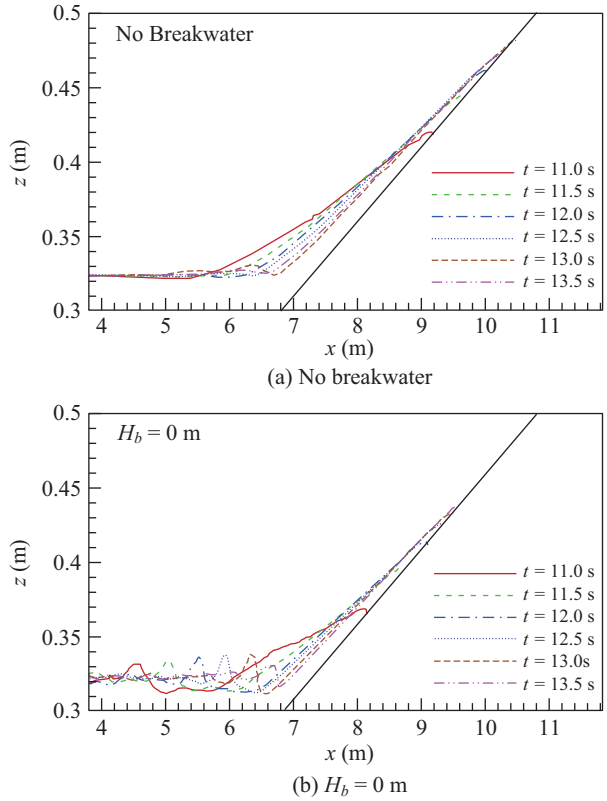

Fig. 6. A comparison between the run-ups of the solitary waves on the slope for (a) no breakwater and (b) when the freeboard of the breakwater (H_b) was 0 m.

3. Velocity Field around Breakwater

The height of the breakwater not only affects the variation of the waveform of the solitary waves but also affects the variation of its velocity field. Figs. 8-10 show the variations of the ensemble-averaged velocity field when the solitary waves propagated over the 3 breakwaters of different heights. Fig. 8 shows the situation involving the submerged breakwater (H_b = –0.04 m). When the wave crest was approaching the upright caisson of the breakwater (t = 5.5 s), the horizontal velocity on top of the caisson increased, and its vertical distribution was almost uniform. When the wave crest passed over the upright caisson (t = 6.0 s), the flow separation occurred at the top-right corner of the upright caisson, due to the changes of the velocity gradient. Additionally, a clockwise circulation was formed at the back of the upright caisson; this vortex was restricted to the area between the top of the berm of the breakwater and the upright caisson.

Fig. 9 shows the situation in which the height of the breakwater was at the still water surface (H_b = 0 m). When the waves propagated over the breakwater (t = 6.0 s, 6.5 s), a slight waterfall occurred in combination with a jet-like flow phenomenon, and there was a clockwise circulation in the area between the top of the berm of the breakwater and the upright caisson. After the jet-like flow occurred, the upward component of the water flow velocity transferred to the downstream

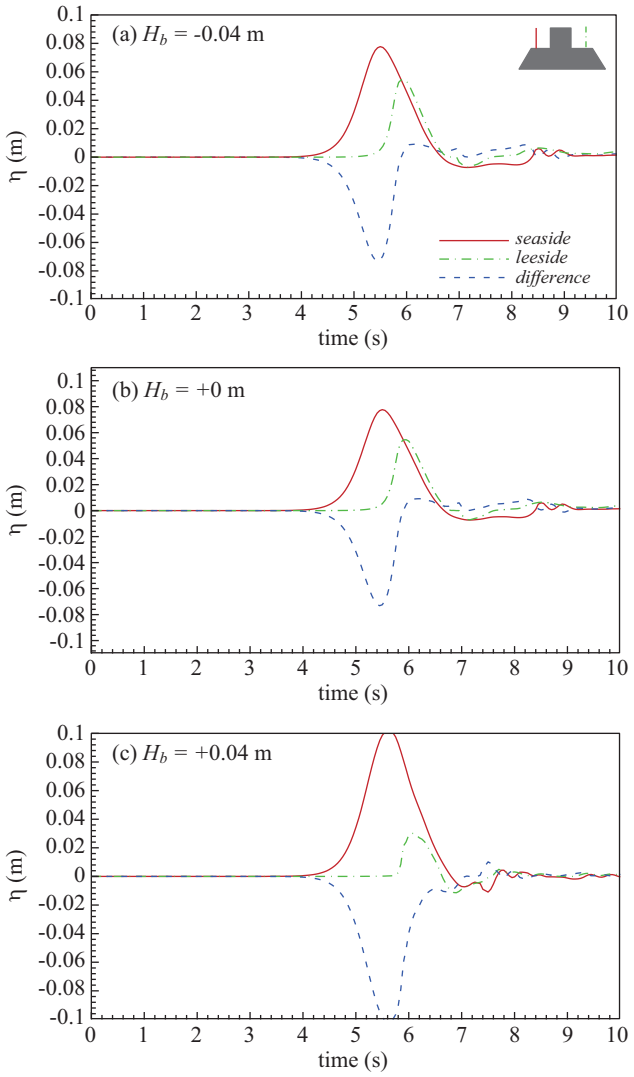

Fig. 7. Comparisons of water level differences between the weather and lee sides of the breakwater when the solitary waves propagated over it.

direction; additionally, a minuscule clockwise vortex was generated near the intersection of the berm and the slope of the foundation.

Fig. 10 shows the situation in which the freeboard of the breakwater (H_b) was +0.04 m. When the solitary waves acted on the breakwater, the water level difference between the weather and lee side was relatively large, which led to the development of significant waterfall and jet-like flow phenomena after the waves propagated over the breakwater; as a result, the jet-like flow almost affected the berm. As described in Mase et al. (2013), the intense jet-like flow might scour the berm if the riprap foundation is relatively high, as a result causing the damage of the breakwater, which was one of the main causes for the damage to the enormous breakwater in Kamaishi Harbor, Japan, during the great tsunami in 2011 (Arikawa et al., 2012). Nevertheless, in breakwater design manuals, protection measures are often only recommended for the seaside berms of break-

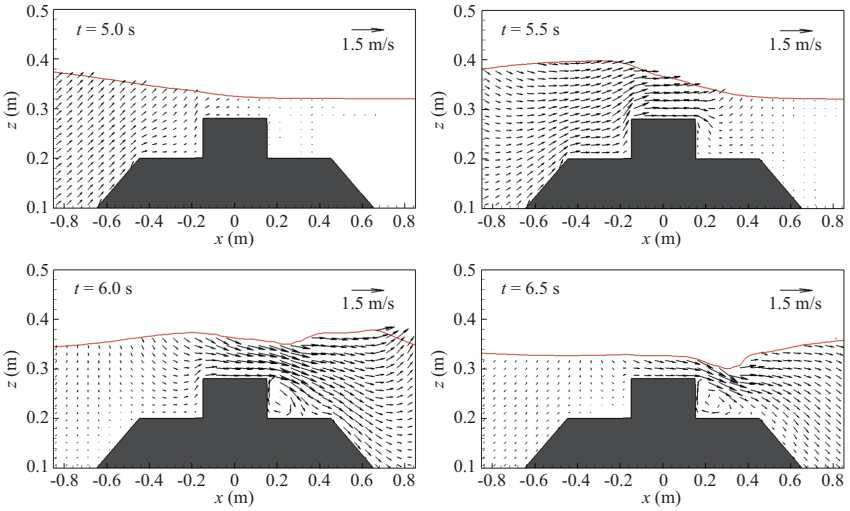

Fig. 8. Ensemble-averaged velocity variation (H_b = -0.04 m) when the solitary waves propagated over the breakwater.

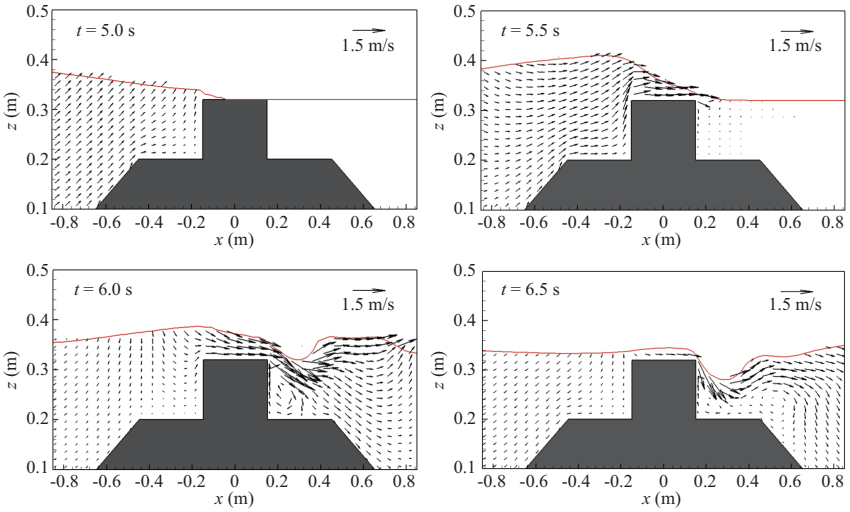

Fig. 9. Ensemble-averaged velocity variation (H_b = 0 m) when the solitary waves propagated over the breakwater.

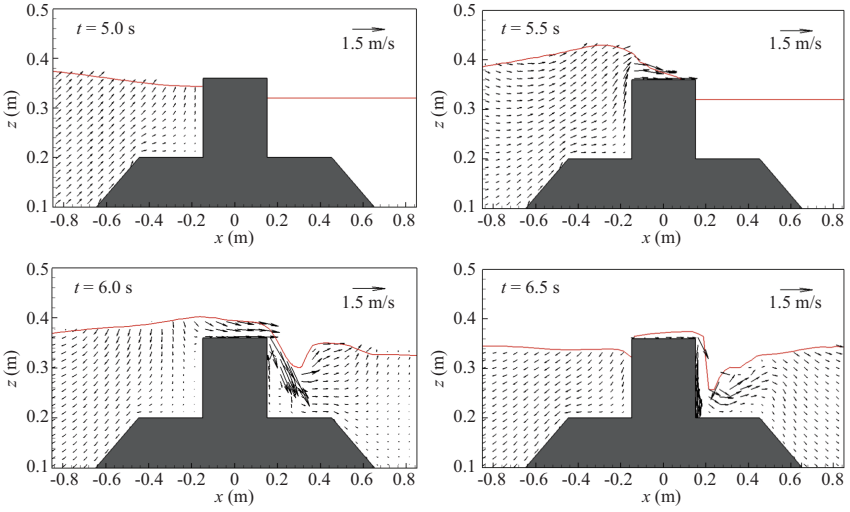

Fig. 10. Ensemble-averaged velocity variation (H_b = +0.04 m) when the solitary waves propagated over the breakwater.

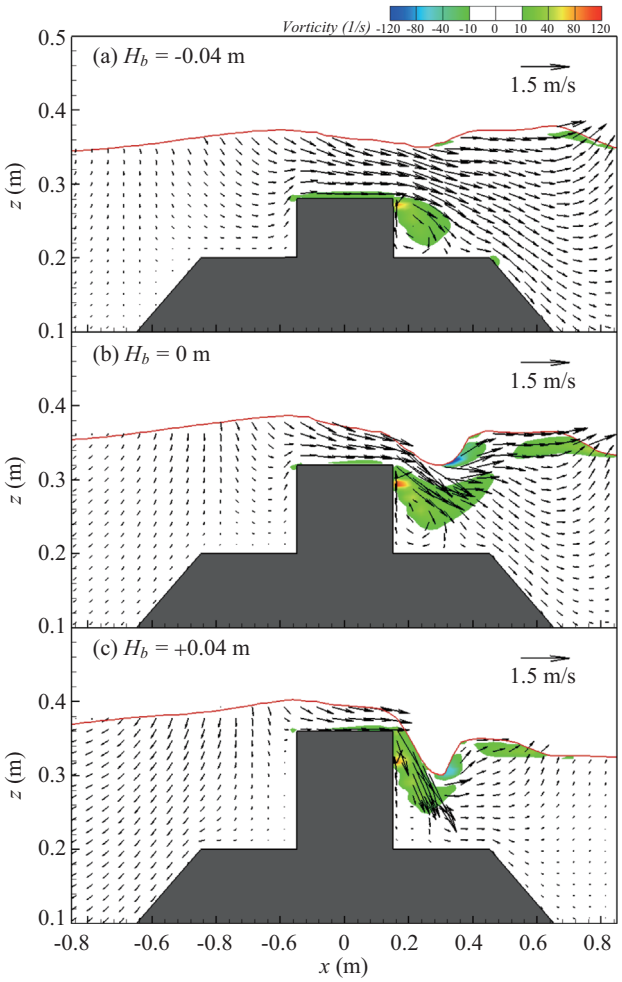

Fig. 11. A comparison among the variations of the vorticities when the solitary waves propagated over the breakwater.

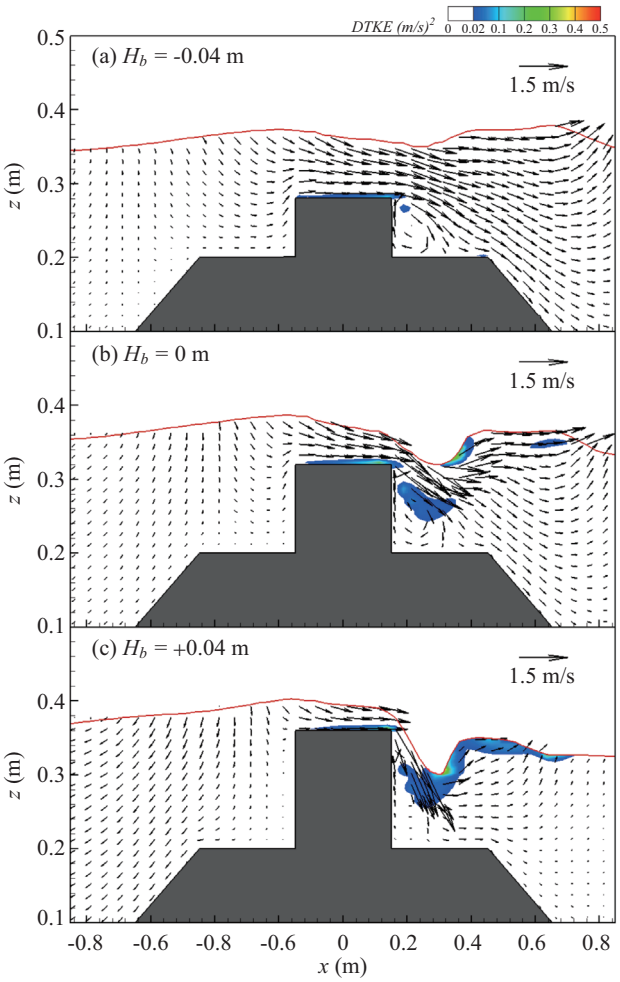

Fig. 12. A comparison among the variations of the turbulent energy dissipation when the solitary waves propagated over the breakwater.

waters and not for the reinforcement of the back berm.

4. Vorticity and Turbulent Energy Dissipation around the Breakwater

The phenomenon of a jet-like flow of various velocities and directions occurred when the solitary waves propagated over the breakwaters. Because a relatively large velocity gradient occurred on the oblique jet-like flow, the vorticity at this location was also relatively significant. However, as the breakwater height increased, the significance of the circulation phenomenon decreased due to the waterfall effect. Fig. 11 shows that when the solitary waves propagated over the breakwater, most of the relatively large vorticities occurred at the inside top corner of the breakwater, as well as the location at which the jet-like flow occurred. However, for the two situations in which $H_b = 0$ m and +0.04 m, negative vorticity occurred at the lowest water surface of the waterfall.

Fig. 12 shows a comparison among the turbulent energy dissipations when the solitary waves propagated over breakwaters of different freeboards. The figure shows that with increasing breakwater height, a relatively large turbulent energy dissipation developed at the jet-like flow and waterfall locations; with the increasing height of the breakwater, the dissipation of turbulent energy occurred over a relatively large area.

5. Run-Up Height Influenced by Breakwater

This section adopts the dimensionless parameters defined in Section 3 for a discussion of the effect of different breakwater heights on the run-up of the solitary waves. Fig. 13 shows the blocking effect of the breakwater on the solitary waves; the wave crest to approach the slope was slower than when no breakwater was present. When the freeboard of the breakwater (H_b) was +0.04 m, the wave crest to approach the slope was the slowest, and after the wave crest propagated over the breakwater, the crest height decreased significantly.

Fig. 14 shows the comparison among the maximum relative run-up heights (η/h_o) for these three breakwater heights and when no breakwater was present. The results show that the maximum run-up height of the solitary waves on the slope decreased with increasing breakwater height. When no breakwater was present, the relative run-up height was $(\eta / h_o)_{\max} = 0.506$. However, when the blocking effect of a breakwater was

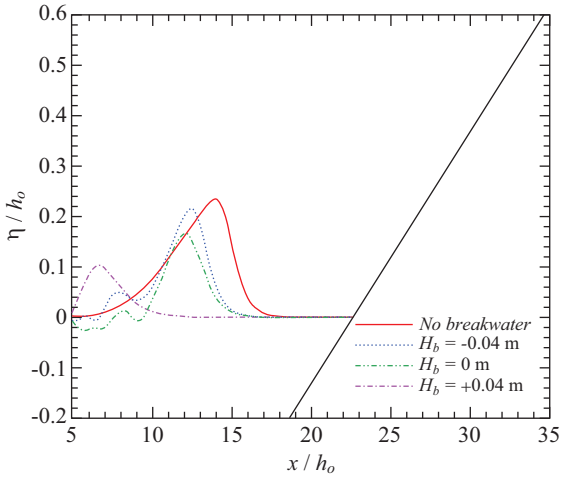

Fig. 13. The effect of different breakwater heights on the propagation of the solitary waves on the slope (t^* = 40).

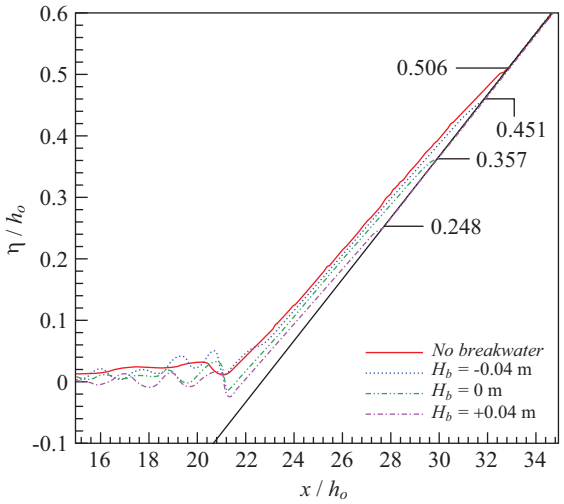

Fig. 14. The effect of different breakwater heights on the run-up height of the solitary waves.

available, the maximum run-up height effectively decreased. In particular for the breakwater with a freeboard (H_b) of +0.04 m, the run-up height effectively decreased by more than one half ($(\eta / h_o)_{max}$ = 0.248). These results demonstrate that the run-up can advance is reduced as the breakwater height increases. However, as mentioned in the previous section, the berm may sustain an impact from a relatively large jet-like flow, as a result of the waterfall phenomenon.

6. Wave Force on Breakwater

Increasing the height of the breakwater can decrease the run-up height of the solitary waves on the slope. However, as the breakwater height is increased, the water level difference between weather and lee side increases as well. This water level difference causes significant changes to the wave force on the breakwater. Fig. 15 shows the variations of the wave

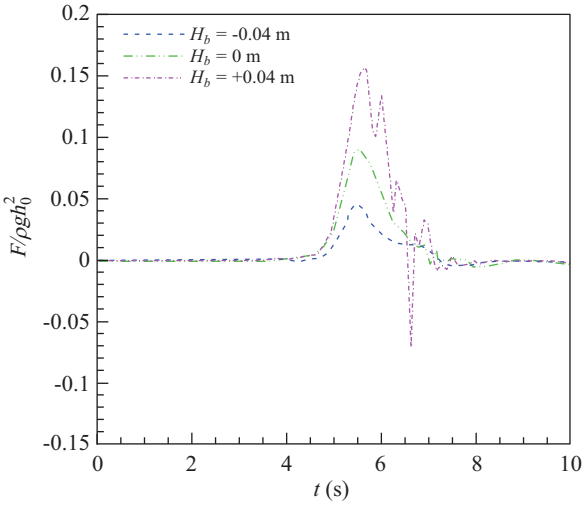

Fig. 15. A comparison among the variations of the wave force when the solitary waves acted on the breakwaters of different heights.

force with respect to the time at which the solitary waves acted on the upright section of breakwaters of various heights. The figure shows that all of the maximum horizontal forces occurred at approximately t = 5.5 s, i.e., when the wave crest of the solitary wave reached the breakwater, the breakwater sustained a relatively large net force. The maximum values of $F / \rho g h_0^2$ for the situations in which H_b = –0.04 m, 0 m and +0.04 m were 0.046, 0.092 and 0.160, respectively, i.e., the maximum wave force when H_b = +0.04 m was 3.5 times that when H_b = –0.04 m and 1.74 times that when H_b = 0 m.

When the top of the breakwater was higher than the water surface, i.e., when H_b = +0.04 m, the maximum wave force was larger than that observed in the other two situations. Additionally, the time variation of the wave force of that breakwater was relatively complicated, in which a negative horizontal force was generated after the waves had propagated over the breakwater. These might have been caused by the jet-like flow that resulted following the overtopping solitary wave and the relatively large waterfall effect.

V. CONCLUSIONS

In the past decades, there have been many numerical and theoretical studies on the run-up of solitary waves and the hydrodynamic characteristics caused by the interaction between solitary waves and structures. In the present study, the RANS model was used to simulate the wave transformations, flow fields and variations of the acting forces of solitary waves propagating over breakwaters of different heights. The numerical simulation results showed that after the solitary waves propagated over the breakwater, the run-up height of the solitary waves propagating along the slope decreased, due to the blocking effect of the breakwater. However, the results also showed that with increasing breakwater height, the water level difference between the weather and leeside of the breakwater

as a result of the solitary waves also increased, which caused the wave force on the breakwater to increase. With respect to flow field variation, when the breakwater was relatively high, after the waves passed over the breakwater, significant waterfall and jet-like flow phenomena occurred; further, such an intense jet-like flow might affect the stability of the riprap berm of the breakwater. The results from this study show that a relatively high breakwater can defer the time available for tsunami waves to reach and run-up land; however, the breakwater itself might also be subject to stability risks.

REFERENCES

Arikawa, T., M. Sato, K. Shimosako, I. Hasegawa, G.-S. Yeom and T. Tomita (2012). Failure mechanism of Kamaishi breakwater due to the great east Japan Earthquake Tsunami. Proceedings of 33rd Conference on Coastal Engineering, Paper No. 33.

Carrier, G. F., T. T. Wu and H. Yeh (2003). Tsunami run-up and draw-down on a plane beach. Journal of Fluid Mechanics 475, 79-99.

Cho, Y. S. and P. L.-F. Liu (1999). Crest length effects in nearshore tsunami run-up around islands. Journal of Geophysical Research 104, 7907-7913.

Choi, B. H., D. C. Kim, E. Pelinovsky and S. B. Woo (2007). Three-dimensional simulation of tsunami run-up around conical island. Coastal Engineering 54, 618-629.

Cooker, M. J., D. H. Peregrine, C. Vidal and J. W. Dold (1990). The interaction between a solitary wave and a submerged semicircular cylinder. Journal of Fluid Mechanics 215, 1-22.

Dentale, F., G. Donnarumma and E. Pugliese Carratelli (2014). Simulation of flow within armour blocks in a breakwater. Journal of Coastal Research 30(3), 528-536.

Flow Science (2012). Flow-3D User Manual. www.flow3d.com.

Grill, S. T., M. A. Losada and F. Martin (1994). Characteristics of solitary wave breaking induced by breakwaters. Journal of Waterway, Port, Coastal, and Ocean Engineering 120(1), 74-92.

Hirt, C. W. and B. D. Nichols (1981). Volume of fluid (VOF) method for dynamics of free boundaries. Journal of Computational Physics 39, 201-225.

Hirt, C. W. and J. M. Sicilian (1985). A porosity technique for the definition of obstacles in rectangular cell meshes. Fourth International Conference on Ship Hydrodynamics, Washington, D.C., September 1985.

Horiguchi, T. and M. Yokota (1968). Report on the survey of the Tokachi Offshore Earthquake Tsunami. Proceedings of 15th Conference on Coastal Engineering, 243-253.

Hsiao, S.-C. and T. C. Lin (2010). Tsunami-like solitary waves impinging and overtopping an impermeable seawall: experiment and RANS modeling. Coastal Engineering 57(1), 1-18.

Huang, C. J. and C. M. Dong (2001). On the interaction of a solitary wave and a submerged dike. Coastal Engineering 43, 265-286.

Jin, J. and B. Meng (2011). Computation of wave loads on the superstructures of coastal highway bridges. Ocean Engineering 38(17-18), 2185-2200.

Li, Y. and F. Raichlen (2003). Energy balance model for breaking solitary wave runup. Journal of Waterway, Port, Coastal, and Ocean Engineering 129(2), 47-59.

Lin, C., T. C. Ho, S. C. Chang, S. C. Hsieh and K. A. Chang (2005). Vortex shedding induced by a solitary wave propagating over a submerged vertical plate. International Journal of Heat Fluid Flow 26, 894-904.

Lin, C., P. H. Yeh, S. C. Hsieh, Y. N. Shih, L. F. Lo and C. P. Tsai (2014). Prebreaking internal velocity field induced by a solitary wave propagating over a 1:10 slope. Ocean Engineering 80, 1-12.

Lin, P. and S. A. S. Karunarathna (2007). Numerical study of solitary wave interaction with porous breakwaters. Journal of Waterway, Port, Coastal, and Ocean Engineering 133(5), 352-363.

Liu, P. L. F., Y. S. Cho, M. J. Briggs, U. Kanoglu and C. E. Synolakis (1995). Runup of solitary waves on a circular island. Journal Fluid Mechanics 302, 259-285.

Liu, P. L. F., H. Yeh and C. E. Synolakis (2008). Advanced Numerical Models for Simulating Tsunami Waves and Runup, In: Advances in Coastal and Ocean Engineering, Vol. 10, World Scientific Pub., Singapore.

Lynett, P. J., P. L. F. Liu, I. J. Losada and C. Vidal (2001). Solitary wave interaction with porous breakwaters. Journal of Waterway, Port, Coastal, and Ocean Engineering 126(6), 314-322.

Lynett, P. J., T. R. Wu and P. L. F. Liu (2002). Modeling wave runup with depth-integrated equations. Coastal Engineering 46(2), 89-107.

Mase, H., Y. Kimura, Y. Yamakawa, T. Yasuda, N. Mori and D. Cox (2013). Were coastal defensive structures completely broken by an unexpectedly large tsunami? – A field survey. Earthquake Spectra 29(S1), S145-S160.

Mori, N. and T. Takahashi (2012). Nationwide post event survey and analysis of the 2011 Tohoku earthquake tsunami. Coastal Engineering Journal 54(1), 1250001.

Nakamura, T., Y. Kuramitsu and N. Mizutani (2008). Tsunami scour around a square structure. Coastal Engineering Journal 50(2), 209-246.

Orszag, S. A., I. Staroselsky, W. S. Flannery and Y. Zhang (1996). Introduction to renormalization group modeling of turbulence. In: Simulation and modeling of turbulent flows, Gatski, T. B., M. Y. Hussaini, and J. L. Lumley, eds., Oxford University Press, 155-183.

Orszag, S. A. and V. Yakhot (1986). Renormalization-Group analysis of turbulence. Physical Review Letter 57, 1722-1724.

Silva, R., I. Losada and M. Losada (2000). Reflection and transmission of tsunami waves by coastal structures. Applied Ocean Research 22(4), 215-223.

Synolakis, C. E. (1987). The runup of solitary waves. J. Fluid Mech., 185, 523-545

Tadepalli, S. and C. E. Synolakis (1994). The run-up of N-Waves on sloping beaches, Proceedings: Mathematical and Physical Sciences 445(1923), 99-112.

Wu, Y. T. and S. C. Hsiao (2013). Propagation of solitary waves on a submerged permeable breakwater. Coastal Engineering 81, 1-18.